Aligned Linear Arrays of Crystalline Nanoparticles

Alison M. Funston,*,[†] Daniel E. Gómez,[‡,§] Matthias Karg,[∥] Kristy C. Vernon,[⊥] Timothy J. Davis,[‡,§] and Paul Mulvaney[∥]

[†]School of Chemistry, Monash University, Clayton, Victoria, 3800, Australia
[‡]CSIRO, Materials Science and Engineering, Private Bag 33, Clayton, Victoria, 3168, Australia
[§]Melbourne Centre for Nanofabrication, Clayton VIC 3168, Australia
[∥]School of Chemistry and Bio21 Institute, University of Melbourne, Parkville, Victoria, 3010, Australia
[⊥]Applied Optics and Nanotechnology Group, Queensland University of Technology, 2 George Street, Brisbane, QLD, 4001, Australia

S Supporting Information

ABSTRACT: Fabrication of one-dimensional arrays of crystalline nanoparticles with tunable particle size and spacing (down to 20 nm) is demonstrated. The individual nanocrystals are pentagonal prisms, and the arrays are up to 11 μm in length, with some arrays containing >50 nanocrystals. Precise particle morphology and interparticle spacing can be maintained down the array. The far-field scattering spectra of the arrays show the near-fields of the nanocrystals are coupled. The method is fast and produces precise, well-defined, coupled plasmonic arrays with optical properties that match well to theory.

SECTION: Plasmonics, Optical Materials, and Hard Matter
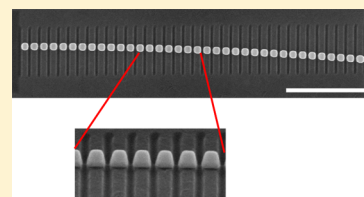
The coupling of the resonances of metallic nanoparticles has emerged as an important area of nanoscience due to the highly enhanced, localized light fields within coupled metal structures. These electromagnetic fields can be used in optoelectronics to confine and guide light within subwavelength dimensions.[1] Linear arrays of nanoparticles are thus promising structures for use within optoelectronics[1-4] and, importantly, single crystalline structures have now been shown to have generally superior optical properties compared to their lithographically fabricated counterparts.[5] The highly crystalline nature and atomically smooth surfaces of metal nanowires significantly increases the propagation length of plasmon excitations (compared to that observed in lithographically fabricated structures) due to a reduction in the far-field scattering.[6,7] However, the arrangement of single-crystal particles into the required linear arrays is nontrivial and remains a fundamental challenge. Most approaches reported to date involve the alignment of presynthesized colloidal crystals using DNA as the linking[8-10] or templating agent[11] and either require complex lithographic techniques, or yield linear arrays in very low yields. The number of particles in the arrays reported using these techniques is generally 1−6, although up to 9 have been reported.[8,11,12]

We report here a new approach to the fabrication of functional metallic nanocrystalline particle arrays. The method is a combination of the top-down and bottom-up approaches to nanofabrication, related to that reported for the fabrication of flat crystalline structures,[5] but in this case is especially optimized for the formation of linear arrays of metal nanocrystals. The crystallinity of the nanoparticles is achieved via chemical synthesis of colloidal silver nanowires, which are modified postsynthetically using focused ion-beam (FIB) milling. Using this approach, linear arrays of >50 nanocrystals

spanning a length of >11 μm have been fabricated. The nanocrystals formed are not flat disks as would be achieved for fabrication from flat crystalline plates, but have a decahedral cross-section characteristic of that of the starting nanowire. The dimensions, longitudinal geometry, and interparticle separation of the nanocrystals in the arrays are easily controlled. The versatility of the technique is proved by also fabricating nanoscale Au nanorod dimers and trimers.

The chemically synthesized Au nanorods and Ag nanowires had a decahedral penta-twinned cross-section. The Ag nanowires were chemically synthesized in an oxygen-free environment using the copper-assisted polyol method.[13] They were washed once with acetone and twice with water to remove excess ligand. The average width of the Ag nanowires was 71 nm with a standard deviation of 17 nm; the lengths of the nanowires were in the micrometer range but varied considerably. Gold nanorods with a high aspect-ratio were prepared via the three-step, seeded-growth method of Murphy et al.[14] They were centrifuged at 2000 rpm for 20 min, followed by decanting of the supernatant and redispersion in water to remove excess ligand and spherical nanoparticles. This was carried out three times to achieve an acceptable yield of high aspect-ratio nanorods. The nanorods and nanowires were dispersed on clean indium tin oxide (ITO)-coated glass slides by spin coating.

Individual Au nanorods and Ag nanowires were identified via scanning electron microscopy (SEM) and then milled using an FIB attached to an FEI Helios 600 D545 SEM. Following
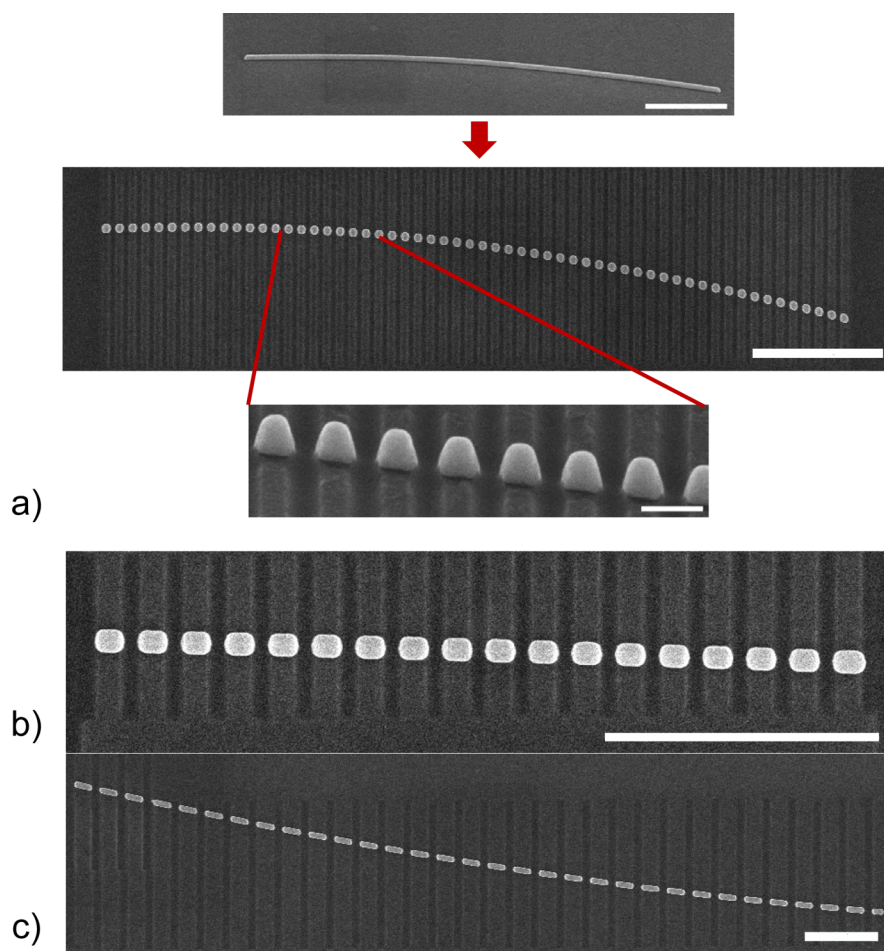
Figure 1. (a) Top: SEM image of a silver nanowire prior to FIB milling taken at 52° to the plane of the substrate. Middle: The nanoparticle array after milling showing the linear array of crystalline nanoparticles and shallow etch marks in the substrate. Bottom: High-resolution image showing the straight sides of the individual nanoparticles (taken at 52° to the plane of the substrate). Scale bar top and middle are 1000 nm, bottom 100 nm. (b) Linear Ag nanocrystal array of 18 nanoparticles with total array length 2.8 μm and average nanoparticle dimensions of length 109 nm, width 84 nm, aspect ratio 1.3, and interparticle separation 52 nm (interparticle separation/length = 0.48). (c) Linear Ag nanocrystal array of 32 nanorods with total array length 11.2 μm and average nanoparticle dimensions of length 249 nm, width 72 nm, aspect ratio 3.4, and interparticle separation 148 nm (interparticle separation/length = 0.61).

fabrication of the arrays, the substrate was marked using the FIB to allow for pattern matching when viewing samples under a darkfield microscope.[15] The scattering spectra of the Au nanorod dimers and trimers were collected on a dark field microscope with a 0.8−0.95 NA dry dark field condenser and a Nikon Plan Fluor ELWD 40x/0.60 NA objective, while the spectra of the arrays were collected with a 1.43−1.2 NA oil-immersion dark-field condensor and a Nikon Plan Fluor 100x/0.5−1.3 NA oil-immersion objective with iris diaphragm. The collected light was focused onto the entrance slit of a MicroSpec 2156i imaging spectrometer coupled to a TE-cooled CCD (Acton Pixis 1024B Excelon). Polarized scattering spectra were collected by rotating a polarizer (LPVIS 100, Thorlabs) in the light path just after the light source. All spectra were collected on ITO glass coverslips in air or immersion oil (RI = 1.515) for index matching as indicated. The scattering spectra were corrected for the small amount of light scattering from the FIB milling marks.

The general procedure is shown in Figure 1a. A nanowire with the desired dimensions and curvature is identified and then milled with a series of linear cuts across the nanowire. The mill depth is set to ensure that the nanowires are completely

milled through, but damage to the substrate is minimized. For the nanoparticle array shown in Figure 1a, the linear array contains 58 nanoparticles, is 5.8 μm long, and very slightly curved. The individual crystalline particles are short penta-twinned prisms. The length of the prisms (the dimension parallel to the interparticle axis) is 67 nm, while their width (edge-to-edge) is 70 nm; based upon the pentagonal cross-section of these crystals, the height is calculated to be 67 nm. These dimensions have a standard deviation of less than 3 nm, well within one pixel of the image. The interparticle separation is 29 nm, again with a standard deviation less than 3 nm, highlighting the high uniformity of the linear arrays produced.

The fabrication of linear arrays with different particle sizes, aspect ratios, and interparticle separations is readily achieved by modifying the FIB milling pattern, and examples are shown in Figure 1a−c and in the Supporting Information in Figures S1 and S2. The interparticle separations in the arrays vary from 20 nm (for Figure S2b) to 200 nm (Figure S2d), while the resulting nanoparticle width is given by the starting width of the respective nanowire. The positional displacement of the nanoparticles (both parallel and perpendicular to the array axis) as well as the nanocrystal shape variation is minimal for
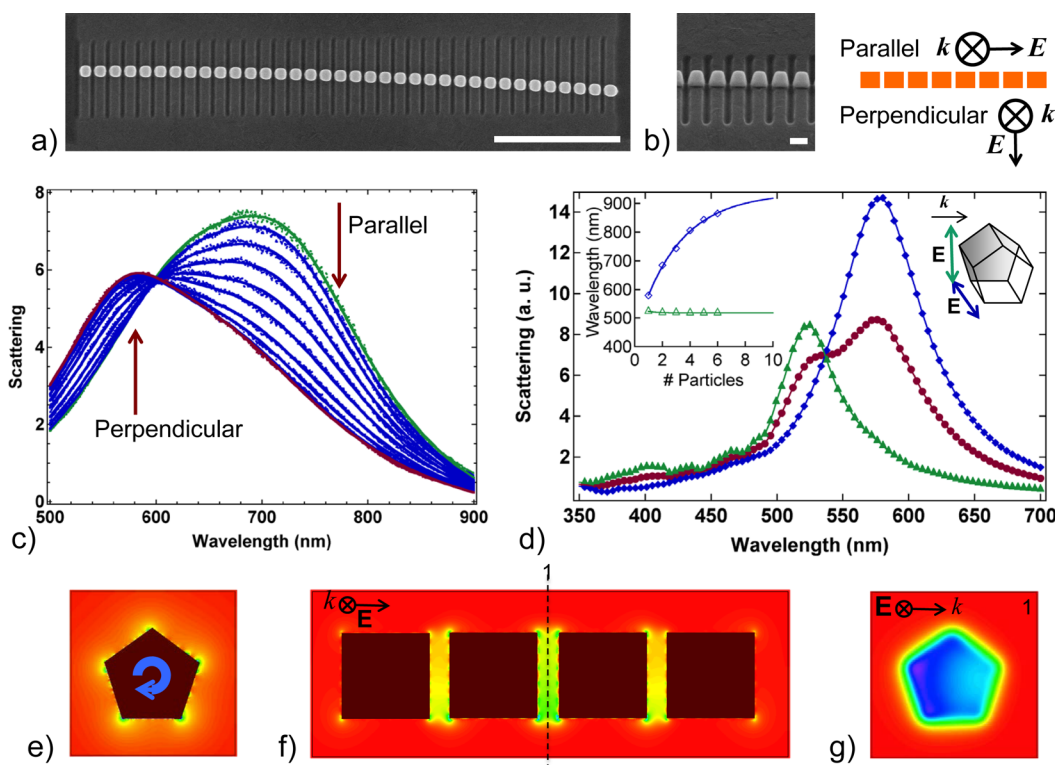
Figure 2. (a) SEM image of linear crystalline array of 36 Ag nanoparticles with total array length 4.3 μm and average nanoparticle dimensions of length = width = 92 nm, aspect ratio 1.0, and interparticle separation 22 nm (interparticle separation/length = 0.24) with the substrate at 90° to the incoming electron beam (scale bar 1000 nm), and (b) substrated tilted by 52° from normal incidence (scale bar 100 nm). (c) Darkfield spectra of the linear array of nanoparticles as a function of polarization. (d) Calculated scattering spectra of a single pentagonal prism (with aspect ratio 1) when the electric field is polarized parallel (blue diamonds) and perpendicular (green triangles) to the C_5 rotation axis as well as for unpolarized light (red spheres). Inset shows the redshift in the longitudinal resonance as a function of number of nanoparticle in the chain (open blue diamonds) and the corresponding blueshift observed for the transverse resonance (open green traingles) for a pentagonal prism with aspect ratio = 1. The number of dipoles used in the simulation was >40 000 per particle, with one dipole per 2.36 nm. (e) Calculated near-field intensity for circularly polarized light perpendicular to the plane of the pentagon and in the center of the nanoparticle. The pentagonal cross-section is superimposed over the intensity distribution to highlight the shape. (f) Calculated near-field intensity of a pentagonal nanoprism tetramer for plane polarized light with electric field oriented parallel to the nanoparticle chain axis. (g) Calculated near-field intensity for plane polarized light with electric field oriented parallel to the nanoparticle chain axis of a pentagonal nanoprism tetramer along cross-section 1 in panel f. Refractive index for experimental data and calculations is uniform due to index matching with $n = 1.515$.

these structures, as described in the Supporting Information, making them promising (in this respect) for use in optoelectronic applications.

The plasmon coupling within the arrays was investigated using dark-field microscopy. In the far-field excitation geometry, all the particles in the chain are excited in phase, and the change in energy of the chain collective resonance mode compared to the localized plasmon resonance of a single, uncoupled particle is related to the $k = 0$ modes of the dispersion relation. The polarized far-field scattering spectra of a linear array of nanoparticles fabricated using FIB milling are shown in Figure 2c along with SEM images of the array (a and b). The individual nanoparticles in this array have an aspect ratio of 1.0. However, due to the pentagonal cross-section of the nanoparticles and the mill pattern used, they are not spherical or plate-like but pentagonal prisms of equal height and width (see inset of Figure 2d for a pictorial representation), indeed, all the nanoparticles created using this method without additional shaping of the ion beam mill pattern are pentagonal prisms. The 5-fold symmetry observed for both silver nanowires and decahedra has been shown to have a large effect on the plasmon modes and thus the optical properties and near-field of the structures.[16−18]

The scattering cross sections of single nanoparticles and arrays were modeled using the discrete dipole approximation (DDA). For these calculations, the program DDSCAT 7.1 was used,[19] with the silver dielectric data of Johnson and Christy[20] and a refractive index of 1.515 to simulate the experimental conditions. The calculated polarized scattering spectra of a single nanoprism are shown in Figure 2d. The spectra are dependent on the polarization of the incoming radiation and a number of modes are predicted. The inherent asymmetry of the pentagonal prisms leads to localization of the near-field at the corners of the pentagon. The localization is shown in Figure 2e for a light vector parallel to the C_5 rotation axis of the pentagonal prism and circularly polarized electric field. This mode is analogous to the azimuthal mode observed for the decahedra; however, for the decahedra the mode is localized at the five central pentagonal base vertices, whereas for these pentagonal prisms it is localized at the five vertices of both the top and bottom faces. For a single pentagonal prism, λ_{max} is calculated to be 524 nm. For excitation with the electric field parallel to the C_5 rotation axis, the plasmon resonance may be considered to be analogous to a longitudinal resonance in a cylinder, and the near-field is concentrated at the flat ends of the prism with $\lambda_{max} = 579$ nm. For a single pentagonal prism,
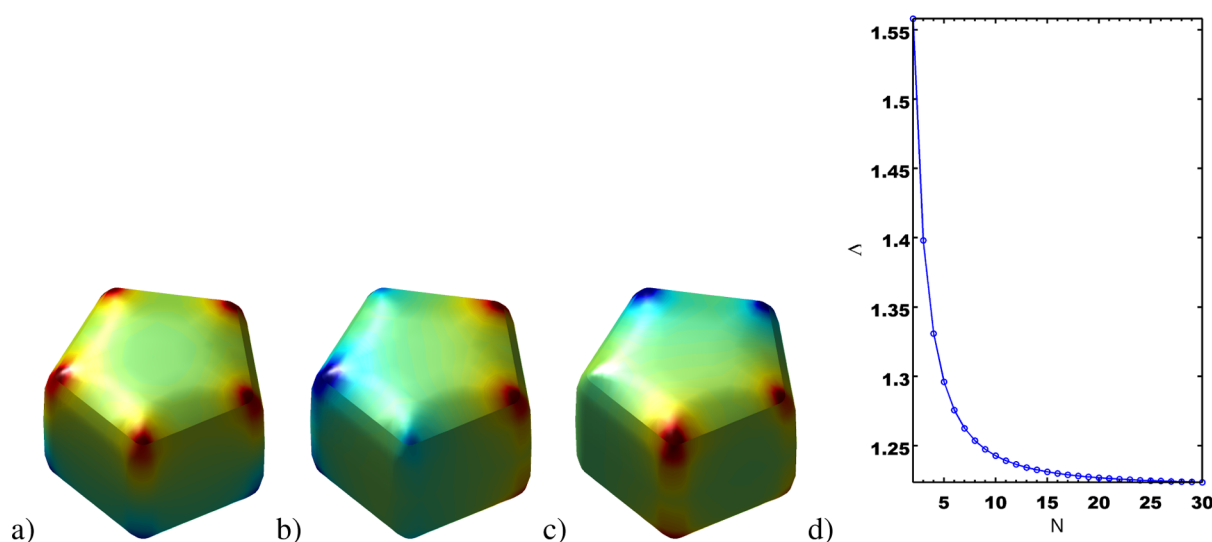
Figure 3. Surface plasmon eigenmodes supported by a pentagon ($L = 92$ nm and $h = 92$ nm); the colors indicate the relative sign of the surface charge with red and blue representing opposite charges. Each eigenmode is characterized by an eigenvalue γ, which has the value 2.15 for mode a, with a dipole moment pointing in the z direction (z is the plane perpendicular to the pentagonal face). For mode b, which has a dipole moment in the plane containing the pentagonal faces, γ is 2.19, whereas for mode c, which has a dipole moment perpendicular to b, γ is 2.30. (d) Evolution of the lowest-energy eigenmode of the particle chain with the number of coupled particles, N, calculated using eq 2 with the experimentally derived value for $C = 1.11$. The dielectric data for Ag was obtained from the literature.[20]

the energy difference between the longitudinal and azimuthal modes is calculated to be 0.22 eV (55 nm). Both the transverse and longitudinal resonances are red-shifted compared to a cylinder of the same volume, and red-shifted compared to the isotropic dipole mode of a sphere of the same volume (see Supporting Information Figure S2).

The individual nanoparticles are arranged in the arrays such that the flat edges face one another. The coupling between nanosphere/nanodisk and nanorod dimers has been investigated in detail previously[8,21−23] and understood using the plasmon hybridization model.[24] The experimentally observed far-field scattering spectra of the array shown in Figure 2a are presented in Figure 2c as a function of polarization of the incoming electric field (from parallel to the nanochain axis to perpendicular to the axis) in increments of 10 degrees. With the electric field of the incoming light polarized parallel to the length of the array (ie interparticle axis), the wavelength of the collective array plasmon resonance is significantly red-shifted with respect to the resonance wavelength calculated for a single prism and $\lambda_{max} = 700$ nm. When the incoming electric field is polarized perpendicular to the long axis of the array, a resonance is obvious at $\lambda_{max} = 574$ nm. A clean isosbestic point is observed at 600 nm. The energy difference between the longitudinal and transverse resonances is 0.39 eV (126 nm), significantly larger than the calculated energy difference between the longitudinal and transverse modes of a single pentagonal prism.

The evolution of the energies of the longitudinal and transverse resonances for 1 up to 6 pentagonal prisms calculated using DDA is shown in the inset to Figure 2d. Consistent with the experimental results, and analogous to the case for a one-dimensional chain of spheres,[8] the longitudinal resonance is calculated to significantly redshift with a progressive increase in the number of nanoparticles in the chain. The redshift may be modeled using an exponential function with $\tau = 3.1$, yielding a plateau at around 10−12 nanoparticles, as observed experimentally and theoretically for

chains of spheres at very small interparticle separations.[8,25−28] The energy of the transverse mode shifts only very slightly as the chain is elongated (inset to Figure 2d). The near-field ($|E|^2$) intensity distribution calculated for the lowest energy mode for all oligomers (electric field parallel to interchain axis) up to 6 nanoparticles is consistent with a longitudinal mode. The intensity of the near-field ($|E|^2$) is greatest in the gap between the central two particles for even numbers of particles, and is greatest in the two gaps either side of the central particle for an odd number of particles. The intensity distribution has a pentagonal cross-section consistent with the shape of the prisms. The calculated near-field intensity ($|E|^2$) for excitation of an Ag pentagonal nanoprism tetramer with the electric field polarized parallel to the nanochain axis is shown in Figure 2f,g. As the number of nanoparticles in the chain increases, there is an increasing contribution to the extinction and scattering cross-section from higher energy, higher-order longitudinal (as well as transverse) modes, although these modes are not resolved in the experimentally determined scattering spectra possibly due to inhomogeneous broadening. The red-shift of the longitudinal resonance observed experimentally is smaller than predicted by the DDA modeling. It is possible that this is due to the small deviation of the end faces of the individual particles from perfectly flat, which would be expected to be more significant for smaller interparticle separation.

In order to gain a semi−quantitative understanding of the surface plasmon modes supported by a N-particle long chain, we adapt here the formalism presented by Barrow et al.,[8] based on the electrostatic eigenmode method.[29] Within this approximation, the optical properties of assemblies of metal nanoparticles are described in terms of their surface plasmon resonance modes, each one characterized by an *eigenvalue* Λ, a dimensionless quantity that determines the value of the resonance wavelength (ω_{SPR}) of the mode through the following relationship between the permittivity of the metal ε_M and that of the surrounding (uniform) medium ε_b:
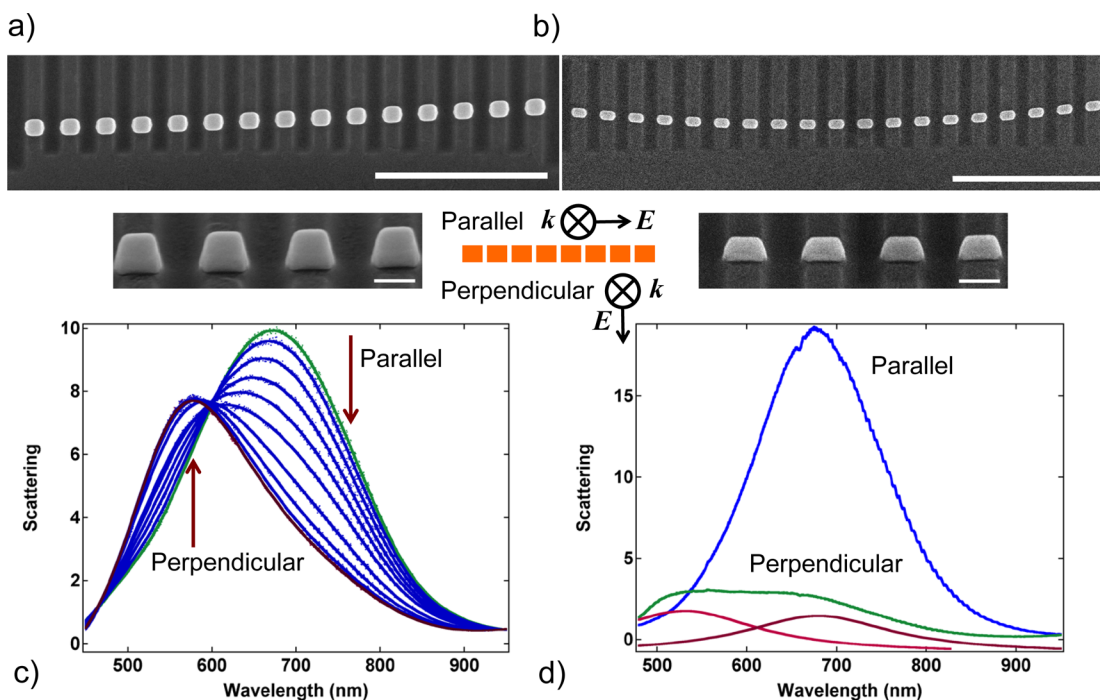
Figure 4. (a) SEM image of linear crystalline array of 15 Ag nanoparticles with total array length 3.0 μm and average nanoparticle dimensions of length = 113 nm, width = 96 nm (aspect ratio 1.2), and interparticle separation 94 nm (interparticle separation/length = 0.83) with the substrate at 90° to the incoming electron beam (scale bar 1000 nm), and tilted by 52° from normal incidence (scale bar 100 nm). (b) SEM image of linear crystalline array of 19 Ag nanoparticles with total array length 2.0 μm and average nanoparticle dimensions of length = 102 nm, width = 62 nm (aspect ratio 1.6), and interparticle separation 89 nm (interparticle separation/length = 0.87) with the substrate at 90° to the incoming electron beam (scale bar 1000 nm), and tilted by 52° from normal incidence (scale bar 100 nm). (c) Darkfield spectra of the linear array of nanoparticles shown in panel a as a function of polarization from parallel (0° with respect to the interparticle axis) to perpendicular (90° with respect to the interparticle axis). (d) Darkfield spectra of the linear array of nanoparticles shown in panel b for parallel (0° with respect to the interparticle axis, blue) and perpendicular polarization (90° with respect to the interparticle axis, green). Red and pink curves are the deconvolution of the perpendicular data to show the contributions from the individual resonance peaks. Refractive index for experimental data is uniform due to index matching with n = 1.515.

$$\mathrm{Re}\,\varepsilon(\omega_{\mathrm{SPR}}) = \varepsilon_{\mathrm{b}}\frac{1 + \Lambda}{1 - \Lambda} \qquad (1)$$

We assume that in the N-nanoparticle chains, the leading term in the interparticle interactions is of the dipole−dipole form and consider only nearest-neighbor coupling. Within this approximation we have found that the eigenvalue Λ_N, which fixes the frequency (wavelength) of the surface plasmon resonance is given by a simple analytical expression, which involves the dipole−dipole coupling constant C and the length of the chain N:

$$\frac{1}{\Lambda_N} = \frac{1}{\gamma} + \frac{C}{\pi}\cos\left(\frac{\pi}{N + 1}\right) \qquad (2)$$

where γ is the eigenvalue of the dipole mode of the non-interacting nanoparticles.

This equation correctly predicts that when N approaches infinity, the surface plasmon resonance wavelength reaches an asymptotic value that is controlled by the geometry of the individual particles (through the parameter γ), the magnitude of coupling constant C, and the dielectric constant of the uniform surrounding medium ε_{b}, parameters that are inter-related according to[8]

$$\varepsilon_{\mathrm{M}}(\lambda_N) = \varepsilon_{\mathrm{b}} \times \frac{1 + \gamma(C/\pi + 1)}{1 + \gamma(C/\pi - 1)} \qquad (3)$$

where ε_{M} is the permittivity of the metal and λ_N the resonance wavelength of a single particle.

For a single pentagon (side = 92 nm and height = 92 nm), the electrostatic eigenmode method predicts that only the first three eigenmodes are bright (have a net dipole moment) and have the surface charge distributions and eigenvalues shown in Figure 3a−c.

For the nanoparticle chain, we measured a plasmon resonance at 700 nm, which we assign to a collective longitudinal plasmon mode. This mode corresponds to an eigenvalue Λ = 1.32. $[\Lambda = (\varepsilon_{\mathrm{Au}}(700\ \mathrm{nm}) - \varepsilon_{\mathrm{b}})/(\varepsilon_{\mathrm{Au}}(700\ \mathrm{nm}) + \varepsilon_{\mathrm{b}})]$,[30] and according to eq 3, this collective longitudinal plasmon mode results from coupling (C = 1.11) between the lowest-energy eigenmodes (a) of each particle in the long chains. The predicted evolution of the eigenmode (and implicitly of the resonance wavelength) with the number N of particles in the chain is shown in Figure 3d), where a clear plateau is exhibited.

The observed trends may be compared to the analogous trends for coupled spheres and cylinders (with aspect ratio 1) with the same interparticle separation and particle volume. The magnitudes of the calculated energy shift for the longitudinal mode of a coupled tetramer chain (compared to the resonance energy of the free particle) are very similar as modeled via DDA, but there is a small absolute energy difference with cylinders > pentagonal cylinders > spheres (see Supporting Information Figure S3). Despite the similarity in the magnitude

of the energy shift, generally the energy of the resonance modes of the coupled pentagonal prisms and cylinders is significantly lower than that of the spheres. This is expected because for these chains, the coupling matrix is algebraically identical for all of these cases. The energy offset arises due to differences in energy of the individual particles (sites) in the chain for the different particle geometries. The calculated $|E|^2$ for the coupled pentagonal prisms and cylinders are higher than for the spheres.

The far-field scattering spectra of arrays with more elongated "rod-like" nanoparticles are shown in Figure 4. The nanorods are aligned end-to-end, a geometry that has been shown to display strong plasmon coupling[22,31] and for which a greater energy difference between the longitudinal and transverse modes would be expected. The individual nanoparticles of the array shown in Figure 4a have an aspect ratio of 1.2, while those within the array in Figure 4b have an aspect ratio of 1.6. The number of individual nanoparticles in both arrays is >12, and the interparticle separation/prism length of both arrays are similar, 0.83 and 0.87 respectively, although the width of the individual nanoprisms and therefore their volumes are quite different. It is well-known that interparticle coupling is dependent upon the interparticle separation. The greater interparticle separation of the individual nanoparticles shown in Figure 4a compared to those in the array shown in Figure 2a is, however, compensated for by the slightly higher aspect ratio of the nanoprisms in Figure 4a and the energy difference between the longitudinal and transverse array resonances for this array (0.33 eV) is only slightly less than that observed for the array in Figure 2a. Further elongation of the nanoparticles (keeping the ratio of interparticle separation/nanoparticle length approximately constant) results in a greater energy difference between the longitudinal and transverse resonances of the array (0.51 eV) as shown in Figure 4a. Note that in these calculations, the effects of retardation have been neglected. Importantly, these micrometer long chains still scatter in the visible region of the spectrum.

To highlight the versatility of the FIB milling of chemically synthesized nanocrystals, Au nanorod dimer and trimer structures were milled from high aspect-ratio Au nanorods (the initial lengths of the nanorods milled varied from 150 to 330 nm). The resulting structures, along with their experimentally determined scattering spectra are shown in Figure 5. The scattering cross-section of the Au dimer and trimer as calculated using DDA (using Weaver's gold dielectric data[32] corrected for surface damping[33] and in an environment with an average refractive index of 1.28[34]) agree well with the experimentally determined spectra (Figure 5). The interaction of asymmetric nanorods is geometry and distance dependent[22,31] and with the nanorods aligned end-to-end the longitudinal plasmon resonances interact in a manner analogous to a bonding interaction,[22,24,31,35,36] resulting in a red-shift of the plasmon resonance of the coupled particle system when compared to the uncoupled nanocrystals. The resonance energy of a single, uncoupled nanorod of the same dimensions as those of the coupled nanorods in the dimer in Figure 5 is calculated to be 915 nm. The calculated spectrum for the coupled system agrees well with the experimentally determined spectrum with a plasmon resonance of 990 nm, giving a red-shift of 75 nm for the coupled system when compared to the uncoupled nanorods.

The trimer structure milled from a high aspect ratio crystalline nanorod is relatively symmetric, with two shorter nanorods at each end and a longer nanorod in the center of the
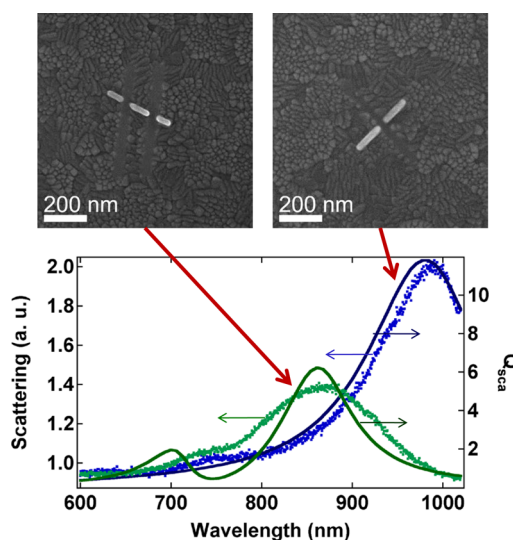
Figure 5. SEM images and scattering spectra (green and blue, left axis) along with DDA calculated spectra (black, right axis) of an Au nanorod dimer and trimer fabricated by FIB milling of presynthesized crystalline nanorods. The dimensions of the two individual nanorods in the dimer are 149 and 138 nm in length and with a width of 33 nm, giving aspect ratios of 4.7 and 4.2, respectively. Their interparticle separation is 31 nm, well within one length of the nanorods. The nanorods were modeled in the DDA simulations as two nanorods each with an aspect ratio of 4.4, the simulation employed 4037 dipoles for each nanorod giving one dipole every 3.0 nm. The nanorods in the trimer have lengths of 84, 103, and 73 nm with a width of 27 nm (aspect ratios of 3.1, 4.0 and 2.6); these were modeled in the DDA simulations as three nanorods with aspect ratios of 2.9, 4.0, and 2.9 for each rod, respectively, giving one dipole every 3.4 nm.

structure. The plasmon coupling within this trimer structure was modeled assuming the end nanorods were approximately equal in length (and therefore aspect ratio) with a longer central nanorod. The plasmon resonance of the uncoupled longer nanorod calculated via DDA had a longitudinal plasmon resonance of 816 nm, while in the coupled structure the wavelength of the lowest energy resonance was 868 nm. The DDA calculations agree well with the experimentally determined spectra. The trimer structure consisted of the smallest particles milled using the FIB method and highlights a number of aspects of the method. Within the course of this work, a number of structures with individual nanoparticle dimensions smaller than the trimer were attempted. While this did result in trimer structures with a discrete number of crystalline nanoparticles, it was observed that the individual nanoparticles became misshapen, and appeared slightly bent downward toward the milled lines. This effect was exacerbated if the original nanorods were sitting on uneven areas of the substrate. Thus the practical size limit for this method is given by a combination of the ion-beam resolution and the intended nanoparticle size. For the experiments here the smallest interparticle gap achieved was 20 nm, and it was found the method is generally not suitable for fabrication of particles <50 nm in length.

In conclusion, the FIB milling of chemically synthesized metal nanowires and nanorods is a convenient method to fabricate highly uniform, linear arrays of crystalline nanoparticles with tunable nanocrystal size and spacing. The near-fields of the individual nanoparticles couple along the length of the nanoparticle chains, making them promising for use in

optoelectronic applications. Investigation of the waveguiding ability and efficiency of these single crystal nanoparticle waveguides is currently underway.

■ ASSOCIATED CONTENT

Ⓢ Supporting Information

Linear arrays fabricated with different particle sizes, aspect ratios, and interparticle separations. Structural descriptions and uniformity information. Evolution of longitudinal and transverse plasmon resonance as a function of number of particles for pentagonal prisms, cylinders, and spheres calculated via DDA. This material is available free of charge via the Internet at http://pubs.acs.org

■ AUTHOR INFORMATION

Corresponding Author
*E-mail: alison.funston@monash.edu.

Notes
The authors declare no competing financial interest.

■ ACKNOWLEDGMENTS

■ REFERENCES

(1) Maier, S. A.; Kik, P. G.; Atwater, H. A.; Meltzer, S.; Harel, E.; Koel, B. E.; Requicha, A. A. G. Local Detection of Electromagnetic Energy Transport Below the Diffraction Limit in Metal Nanoparticle Plasmon Waveguides. *Nat. Mater.* **2003**, *2*, 229−232.

(2) Quinten, M.; Leitner, A.; Krenn, J. R.; Aussenegg, F. R. Electromagnetic Energy Transport via Linear Chains of Silver Nanoparticles. *Opt. Lett.* **1998**, *23*, 1331−1333.

(3) Brongersma, M. L.; Hartman, J. W.; Atwater, H. A. Electromagnetic Energy Transfer and Switching in Nanoparticle Chain Arrays Below the Diffraction Limit. *Phys. Rev. B* **2000**, *62* (R16), 356−359.

(4) Maier, S. A.; Brongersma, M. L.; Kik, P. G.; Meltzer, S.; Requicha, A. A. G.; Atwater, H. A. Plasmonics - A Route to Nanoscale Optical Devices. *Adv. Mater.* **2001**, *13*, 1501−1505.

(5) Huang, J. S.; Callegari, V.; Geisler, P.; Bruning, C.; Kern, J.; Prangsma, J. C.; Wu, X.; Feichtner, T.; Ziegler, J.; Weinmann, P.; Kamp, M.; Forchel, A. Atomically Flat Single-Crystalline Gold Nanostructures for Plasmonic Nanocircuitry. *Nat. Commun.* **2010**, *1*, 150.

(6) Ditlbacher, H.; Hohenau, A.; Wagner, D.; Kreibig, U.; Rogers, M.; Hofer, F.; Aussenegg, F. R.; Krenn, J. R. Silver Nanowires as Surface Plasmon Resonators. *Phys. Rev. Lett.* **2005**, *95*, 257403.

(7) Wiley, B. J.; Lipomi, D. J.; Bao, J.; Capasso, F.; Whitesides, G. M. Fabrication of Surface Plasmon Resonators by Nanoskiving Single-Crystalline Gold Microplates. *Nano Lett.* **2008**, *8*, 3023−3028.

(8) Barrow, S. J.; Funston, A. M.; Gómez, D. E.; Davis, T. J.; Mulvaney, P. Surface Plasmon Resonances in Strongly Coupled Gold Nanosphere Chains from Monomer to Hexamer. *Nano Lett.* **2011**, *11*, 4180−4187.

(9) Barrow, S. J.; Wei, X.; Baldauf, J. S.; Funston, A. M.; Mulvaney, P. The Surface Plasmon Modes of Self-Assembled Gold Nanocrystals. *Nat. Commun.* **2013**, *3*, 1275.

(10) Barrow, S. J.; Funston, A. M.; Wei, X.; Mulvaney, P. DNA-Directed Self-Assembly and Optical Properties of Discrete 1D, 2D and 3D Plasmonic Structures. *Nano Today* **2013**, *8*, 138−167.

(11) Lalander, C.; Zheng, Y.; Dhuey, S.; Cabrini, S.; Bach, U. DNA-Directed Self-Assembly of Gold Nanoparticles onto Nanopatterned Surfaces: Controlled Placement of Individual Nanoparticles into Regular Arrays. *ACS Nano* **2010**, *4*, 6153−6161.

(12) Chen, H.-Y.; He, C.-L.; Wang, C.-Y.; Lin, M.-H.; Mitsui, D.; Eguchi, M.; Teranishi, T.; Gwo, S. Far-Field Optical Imaging of a Linear Array of Coupled Gold Nanocubes: Direct Visualization of Dark Plasmon Propagating Modes. *ACS Nano* **2011**, *5*, 8223−8229.

(13) Korte, K. E.; Skrabalak, S. E.; Xia, Y. Rapid Synthesis of Silver Nanowires through a CuCl- or CuCl$_2$-mediated Polyol Synthesis. *J. Mater. Chem.* **2008**, *18*, 437−441.

(14) Busbee, B. D.; Obare, S. O.; Murphy, C. J. An Improved Synthesis of High-Aspect-Ratio Gold Nanorods. *Adv. Mater.* **2003**, *15*, 414−416.

(15) Novo, C.; Funston, A. M.; Pastoriza-Santos, I.; Liz-Marz'an, L. L.; Mulvaney, P. Spectroscopy and High-Resolution Microscopy of Single Nanocrystals by a Focused Ion Beam Registration Method. *Angew. Chem. Int. Ed.* **2007**, *46*, 3517−3520.

(16) Song, M.; Bouhelier, A.; Bramant, P.; Sharma, J.; Dujardin, E.; Zhang, D.; Colas-des Francs, G. Imaging Symmetry-Selected Corner Plasmon Modes in Penta-twinned Crystalline Ag Nanowires. *ACS Nano* **2011**, *5*, 5874−5880.

(17) Myroshnychenko, V.; Nelayah, J.; Adamo, G.; Geuquet, N.; Rodríguez-Fernández, J.; Pastoriza-Santos, I.; MacDonald, K. F.; Henrard, L.; Liz-Marzán, L. M.; Zheludev, N. I.; Kociak, M.; de Abajo, F. J. G. Plasmon Spectroscopy and Imaging of Individual Gold Nanodecahedra: A Combined Optical Microscopy, Cathodoluminescence, and Electron Energy-Loss Spectroscopy Study. *Nano Lett.* **2012**, *12*, 4172−4180.

(18) Rodríguez-Fernández, J.; Novo, C.; Myroshnychenko, V.; Funston, A. M.; Sánchez-Iglesias, A.; Pastoriza-Santos, I.; Pérez-Juste, J.; Abajo, F. J. G. d.; Liz-Marzán, L. M.; Mulvaney, P. Spectroscopy, Imaging and Modeling of Individual Gold Decahedra. *J. Phys. Chem. C* **2009**, *113*, 18623−18631.

(19) Draine, B. T.; Flatau, P. J. User Guide to the Discrete Dipole Approximation Code DDSCAT 7.1. http://arxiv.org/abs/1002.1505, 2010.

(20) Johnson, P. B.; Christy, R. W. Optical Constants of the Noble Metals. *Phys. Rev. B* **1972**, *6*, 4370−4379.

(21) Gunnarsson, L.; Rindzevicius, T.; Prikulis, J.; Kasemo, B.; Kall, M.; Zou, S. L.; Schatz, G. C. Confined Plasmons in Nanofabricated Single Silver Particle Pairs: Experimental Observations of Strong Interparticle Interactions. *J. Phys. Chem. B* **2005**, *109*, 1079−1087.

(22) Funston, A. M.; Novo, C.; Davis, T. J.; Mulvaney, P. Plasmon Coupling of Gold Nanorods at Short Distances and in Different Geometries. *Nano Lett.* **2009**, *9*, 1651−1658.

(23) Tamaru, H.; Kuwata, H.; Miyazaki, H. T.; Miyano, K. Resonant Light Scattering from Individual Ag Nanoparticles and Particle Pairs. *Appl. Phys. Lett.* **2002**, *80*, 1826−1828.

(24) Prodan, E.; Radloff, C.; Halas, N. J.; Nordlander, P. A Hybridization Model for the Plasmon Response of Complex Nanostructures. *Science* **2003**, *302*, 419−422.

(25) Sweatlock, L. A.; Maier, S. A.; Atwater, H. A.; Penninkhof, J. J.; Polman, A. Highly Confined Electromagnetic Fields in Arrays of Strongly Coupled Ag Nanoparticles. *Phys. Rev. B* **2005**, *71*, 7.

(26) Harris, N.; Arnold, M. D.; Blaber, M. G.; Ford, M. J. Plasmonic Resonances of Closely Coupled Gold Nanosphere Chains. *J. Phys. Chem. C* **2009**, *113*, 2784−2791.

(27) Citrin, D. S. Plasmon Polaritons in Finite-Length Metal-Nanoparticle Chains: The Role of Chain Length Unravelled. *Nano Lett.* **2005**, *5*, 985−989.

(28) Willingham, B.; Link, S. Energy Transport in Metal Nanoparticle Chains via Sub-radiant Plasmon Modes. *Opt. Express* **2011**, *19*, 6450−6461.

(29) Davis, T. J.; Gómez, D. E.; Vernon, K. C. Simple Model for the Hybridization of Surface Plasmon Resonances in Metallic Nanoparticles. *Nano Lett.* **2010**, *10*, 2618−2625.

(30) Davis, T. J.; Vernon, K. C.; Gómez, D. E. Designing Plasmonic Systems Using Optical Coupling Between Nanoparticles. *Phys. Rev. B* **2009**, *79*, 155423.

(31) Funston, A. M.; Davis, T. J.; Novo, C.; Mulvaney, P. Coupling Modes of Gold Trimer Superstructures. *Philos. Trans. R. Soc. A* **2011**, *369*, 3472−3482.

(32) Weaver, J.; Krafka, C.; Lynch, D.; Koch, E. *Physics Data: Optical Properties of Metals, Part 2: Noble Metals, Aluminium, Scandium, Yttrium, the Lanthanides and the Actinides*; Fach-Informations Zentrum: Karlsruhe, Germany, 1981.

(33) Félidj, N.; Aubard, J.; Lévi, G. Discrete Dipole Approximation for Ultraviolet-Visible Extinction Spectra Simulation of Silver and Gold Colloids. *J. Chem. Phys.* **1999**, *111*, 1195−1205.

(34) Novo, C.; Funston, A. M.; Pastoriza-Santos, I.; Liz-Marzán, L. M.; Mulvaney, P. Influence of the Medium Refractive Index on the Optical Properties of Single Gold Triangular Prisms on a Substrate. *J. Phys. Chem. C* **2008**, *112*, 3−7.

(35) Nordlander, P.; Oubre, C.; Prodan, E.; Li, K.; Stockman, M. I. Plasmon Hybridization in Nanoparticle Dimers. *Nano Lett.* **2004**, *4*, 899−903.

(36) Myroshnychenko, V.; Rodríguez-Fernández, J.; Pastoriza-Santos, I.; Funston, A. M.; Novo, C.; Mulvaney, P.; Liz-Marzán, L. M.; de Abajo, F. J. G. Modelling the Optical Response of Gold Nanoparticles. *Chem. Soc. Rev.* **2008**, *37*, 1792−1805.